Atmos. Chem. Phys. Discuss., 6, 9003–9032, 2006
www.atmos-chem-phys-discuss.net/6/9003/2006/

Atmospheric Chemistry and Physics Discussions

Solid particles in the tropical lowest stratosphere

J. K. Nielsen[1], N. Larsen[1], F. Cairo[2], G. Di Donfrancesco[3], J. M. Rosen[4], G. Durry[5,7], G. Held[6], and J. P. Pommereau[7]

[1]Danish Meteorological Institute, Lyngbyvej 100, 2100 Kbh. Ø, Denmark
[2]Institute for Atmospheric Science and Climate, CNR, Via del Fosso del Cavaliere 100, 00133 Rome, Italy
[3]Italian National Agency for New Technologies, Energy and Environment, ENEA C. R. Cassaccia, Via Anguillarese 301, 00060 Rome, Italy
[4]University of Wyoming, Department of Physics and Astronomy, Laramie, Wyoming 82071
[5]Groupe de Spectrometrie Moleculaire et Atmospherique, CNRS, Universite de Reims , 51687 Reims, France
[6]Instituto de Pesquisas Meteorológicas, Universidade Estadual Paulista, CX Postal, 281 17015-970 BAURU, S.P., Brasil
[7]CNRS, Institut Pierre Simon Laplace, Service d'Aeronomie, B.P. 3, 91371 Verrieres le Buisson Cedex, France

Received: 1 June 2006 – Accepted: 24 July 2006 – Published: 25 September 2006

Correspondence to: J. K. Nielsen (jkn@dmi.dk)

Abstract

We report in situ and remote observations proving occasional occurrence of solid particles in the tropical lowest stratosphere, far away from deep convective events. The particles were found during field campaigns in Southeast Brazil (49.03 W 22.36 S). They occur in the altitude range from 17.5 to 20.8 km, at temperatures up to at least 10 K above the expected frost point temperature. While stability of ice particles at these altitudes is unexpected from a theoretical point of view, it is argued that these observations are indications of tropospheric air masses penetrating into the stratosphere during convective overshoots. It is concluded that the intrusion of tropospheric air must have carried a large amount of water with it, which effectively hydrated the lowest stratosphere, and consequently suppressed sublimation. This conclusion is further supported by a separate water vapor mixing ratio profile obtained at the same observation site.

1 Introduction

In the global tropospheric-stratospheric mass exchange pattern, known as the Brewer Dobson circulation, air enters the stratosphere mainly through the tropical tropopause (Holton et al., 1995). During ascent through the Upper Troposphere/Lower Stratosphere (UTLS) air masses loose most of their water content through sedimentation of ice particles at the extremely cold temperatures near the tropopause. The detailed mechanisms of this dehydration, or "freeze drying" process are of great importance for understanding the stratospheric water budget.

Two main paradigms can be identified in the ongoing discussion about the nature of the dehydration processes. In the first paradigm, dehydration happens as a slow large-scale process where air masses are transported through the cold point tropopause on their way to the stratosphere. Newell and Gould-Stewart (1981) pointed at the tropopause over the Maritime Continent as the place where air probably enters the stratosphere and is dehydrated. They noted that the temperature at the maritime

tropopause at 190.8 K correlates with a stratospheric water content of 3.5 ppmv.

In the second paradigm, dehydration happens in connection with deep convective systems. Danielsen (1982) proposed that air enters the stratosphere in overshooting turrets of tropical thunderstorms. He suggested that the anvils remaining from deep convective events act as "dehydration engines". Sherwood and Dessler (2001) proposed that air masses penetrate into the so called Tropical Tropopause Layer (TTL, 50–150 hPa) by overshooting convective events. During this process air undergoes dehydration due to extremely low temperatures in the updrafts. In the detrainment from the updraft, air masses are mixed with air masses at the level of detrainment, before they stabilize at a lower level. Thereafter the air proceeds in a very slow ascent through the TTL, where it undergoes further mixing with new convective overshoots.

However, it has been argued from thermodynamic grounds by Folkins et al. (1999) that convective events seldom rise into the TTL. Likewise, Küpper et al. (2004) conclude on the basis of cloud resolving simulations, that vertical transport within overshooting cumulus is insignificant in the TTL. In line with Potter and Holton (1995); Fueglistaler et al. (2004); Hartmann et al. (2001); Gettelman et al. (2000), they conclude that dehydration mainly happens during slow ascent through a cold tropopause. Several studies address the details of this type of process. It has been demonstrated in microphysical simulations by Jensen et al. (2001) how such dehydration may work. Potter and Holton (1995) showed, with a bulk microphysical model, that buoyancy waves generated from convection may form cirrus which enhance dehydration of the lower stratosphere. Hartmann et al. (2001); Holton and Gettelman (2001), as well as Gettelman et al. (2000), pointed out that cirrus residing above convective systems can maintain radiative stability because of anvils shielding the radiation from below. They proposed that air is horizontally advected into extremely cold large areas positioned over convective activity in the western Pacific, and thereby dehydrated. This concept was incorporated into a broader picture by Fueglistaler et al. (2004), showing that air is lifted into the TTL mainly above the western Pacific, and thereafter distributed globally in the TTL, where it circulates for a long time and eventually gets dehydrated as it

passes through the coldest area of the TTL, also over Western Pacific. The analysis of Fueglistaler et al. (2004) was based on ECMWF-trajectories, and it left no importance to convective overshooting as a dehydration mechanism. A similar approach, based on NCEP-trajectories and detailed microphysics (Jensen and Pfister, 2004) also leads to effective dehydration, suggesting a need for an additional water source which could be deep convection.

On the other hand, deep convective penetration into the TTL happens occasionally (Alcala and Dessler, 2002; Adler and Mack, 1986; Ebert and Holland, 1992; Simpson et al., 1993), but it is unclear what the role of such events is with respect to dehydration of air entering into the stratosphere. The question is, whether convective events act like additional dehydration parallel to cooling by slow ascent, or if convective events in fact do hydrate the lower stratosphere. Both cases could include the additional feature of convective events enforcing the dehydration by emission of buoyancy waves, which temporarily may decrease temperatures around the tropopause.

Here we present in-situ and remote measurements of very dilute particle occurrences above the TTL far away from any convective events. We argue that these particles most likely were emitted from a thunderstorm several hours earlier, and we discuss the possible implications for the role of deep convection in the troposphere to stratosphere transport.

2 Data collection and observations

The HIBISCUS (Impact of tropical convection on the upper troposphere and lower stratosphere (UTLS) at global scale) campaigns took place in Bauru, Brazil, in 2001, 2003 and 2004 (Pommereau, 2004). These campaigns included local balloon-borne measurements of aerosols and chemical species and ground-based lidar measurements. Here we present two specific particle observations, supported by a series of ozone soundings and radar observations.

The first observation (O1) was made in situ on 21 February 2004, 01:19 UT at 17.7

to 18.9 km altitude with a balloon-borne Wyoming backscatter sonde during descent. This instrument detects backscatter signals at wavelengths 940 nm and 480 nm (see Rosen and Kjome, 1991 for a technical description of the Wyoming backscatter sonde). Figure 1 shows some details of O1. The backscatter ratio at 940 nm, plotted as a filled red curve, shows values bigger than the background in the altitude range 17.7 to 18.9 km. The observation was done on the descent of one flight out of a total of ten. The fact that the layer was not observed on the backscatter sonde's ascent 22 min earlier suggests that it is of limited horizontal extent. The thick grey line shows the average backscatter ratio above the TTL from all flights including the highlighted one. This proves the existence of particles different from the background aerosols in an altitude range which lies just above the top of the TTL. The temperature (thin black line) in this altitude interval ranges from 195.9 to 202.4 K. To illustrate why this observation is unexpected, we have estimated the frost point temperature (T_{ice}, dashed black line) by assuming a water vapor mixing ratio of 6.06 ppmv. This is the lowest water vapor mixing ratio deduced from the temperature and pressure profiles, by assuming saturation of water vapor with respect to ice. The value of 6.06 ppmv is an overestimate of the water vapor mixing ratio compared to normal values (2–4 ppmv) at the bottom of the stratosphere, and the air parcels above the TTL had probably not passed through the local tropopause in this case. The T_{ice} estimate should be considered as a maximum value for this property, which illustrates why the presence of particles above the TTL is surprising. Air masses at these high altitudes are expected to be subsaturated. The dotted black line is the frost point temperature calculated by assuming a water vapor mixing ratio of 36.1 ppmv, the value corresponding to saturation with respect to ice at 18.9 km. The color index (blue dots in Fig. 1) contains information about particle sizes, which will be discussed further in Sect. 3. O1 is particularly interesting because it was supported by continuous radar observations during the whole mission (Figs. 2 and 3). These radar observations show that there were no deep convective events close to the observation during the launch and ascent (Fig. 2). We shall interpret the implications of this fact in the discussion below.

The second observation (O2, Fig. 4) was done on 14 February 2001, during the HIBISCUS pre-campaign with a ground-based 532 nm μ-lidar (see Di Donfrancesco et al., 2006 for a technical discription of the μ-lidar). In the altitude range 18.8–20.8 km optically thin particle layers were observed. The volume depolarization, which is non-zero from 18.8 km to 21.1 km, indicates that the particles were non-spherical, i.e. solid. This observation is remarkable because the range where particles were observed extends to very high altitudes. The backscatter ratio is also larger than in O1. Generally the backscatter ratio is smaller at 532 nm than at 940 nm, for a given particle distribution, so the larger lidar backscatter ratio indicates larger number density or larger particle radius in O2 than in O1. The horizontal extension of this phenomenon must have been limited, since the signal was only there for a approximately 15 min, corresponding to a horizontal extend of around 10 km. The local meteorological situation was very similar to that of O1. An area of convective activity was located east of Bauru in the early afternoon and the steady easterly in the lowest stratosphere transported airmasses from this region to the area above Bauru at 18–20 km altitude during the early evening when O2 was performed. See Fig. 5. The convective area around Bauru at 16:01 local sun time has nothing to do with the observation. The area from which the observed particles could originate is at the easterly rim of the radar range.

3 Number density and composition

Considering O1, we first note that the increase in color index accompanying the particles around 18–19 km indicates that the particles were larger than the background aerosol (Schreiner et al., 2003). Particle sizes cannot be derived uniquely from the color index, but assuming a log-normal size distribution (stdv 1.5) of ellipsoid ice particles with aspect ratio 1.05, one can make a crude estimate of the median radius. Utilizing the T-matrix method of Mishchenko and Travis (1998), the backscatter ratio and color index for a range of log normal standard deviations and median radius values are mapped in Fig. 6.

From Fig. 1 we see that the high-altitude particles have a color index between 7 and 12. From Fig. 6 we find that it is reasonable to assume that the radius median lies within 0.2–1.5 μm (white ellipse in Fig. 6). Given this radius interval and the measured aerosol backscattering ratio at approximately 2–3, we are lead to conclude that the number density is in the interval $0.4–10\times10^{6}$ (kg air)$^{-1}$ (or 0.03–1/cm^{3}). The particles were most probably solid, since liquid aerosols activated to water droplets of 0.2–1.5 μm would have nucleated and formed ice very quickly. This is also consistent with O2, from which we can conclude directly, based on the volume depolarization signal, that the measured particles were solid. It is possible that the particles were composed of nitric acid tri-hydrate (NAT). Neither ice or NAT are stable in the dry environment above the TTL. In Fig. 7 the ice frost point temperatures and NAT condensation temperatures are plotted for different reasonable assumptions about water vapor and gas phase HNO_3 mixing ratios. We conclude from Fig. 7, that no matter whether the particles at 18.9 km were made of NAT or ice, the air in which they reside would have to be cooled at least 10 K along an isentrope in order to reach saturation, if we assume water vapor and HNO_3 mixing ratios close to lower stratospheric levels. NAT-particles do have a much longer sublimation time than ice particles, so NATparticles would have the ability to remain present in a non-equilibrium state for several hours. This could explain why the particles had not sublimated at the time of observation, but it would still be an open question how these particles were created in – or brought to – the lowest stratosphere. Particle "clouds" with number densities in the order of 10^{-5} cm^{-3} containing NO_y have been observed recently at the tropical cold point tropopause (Popp et al., 2005). The present observations are at higher altitude and the number density is much larger. Assuming that the particles were composed of NAT, we estimate their HNO_3 content to $0.29–4.9\times10^{-9}$ kg (kg air)$^{-1}$, which would correspond to a gas phase mixing ratio of 0.13–2.3 ppbv, if the particles were fully sublimated. This is of course based on the particle radius interval estimated from Fig. 7.

Typical values of gas phase HNO_3 in the tropical tropopause lie around 0.1 ppbv and lower (Popp et al., 2005), which is also the saturation mixing ratio at the temperature

minimum of O1, if one assumes a water vapor mixing ratio of 6.06 ppmv. Thus, for an airmass to form an amount of NAT corresponding to 0.13–2.3 ppbv, it would require an unexplained abnormally high HNO_3 abundance during the nucleation and growth of NAT particles. In any case it is not necessary to assume that the particles were composed of NAT in order to explain their occurrence. In the following analysis we assume that the particles were made of ice.

4 Discussion

4.1 Origin of high altitude particles

The most striking feature of O1 is that there is no sign of local deep convection in the radar images close to the time of observation, as seen in Fig. 2. This makes the particle occurrences somewhat mysterious. We neglect the quite unlikely possibility that the particles were traces of meteorites originating from outside the earth's atmosphere. Such a highly localized event would not leave traces in a large vertical range (note that there is strong shear motion around both measurements). Likewise it seems unlikely that the particles are traces of volcanic eruptions, which presumably would have resulted in a smooth layer of great extent. We are therefore led to consider two possibilities for the origin of the particles detected in O1, namely gravity waves or deep convective outflow.

Suppose that gravity waves of short wavelength had decreased the temperature locally, so that some air parcels in the lowest stratosphere became sufficiently supersaturated with respect to ice for ice nucleation to occur. This is similar to the mechanism proposed by Potter and Holton (1995). We can estimate that a temperature drop of more than 10 K would be required in order to reach the ice nucleation temperature. The ice nucleation temperature lies a few Kelvin below the frost point (dashed line in Fig. 1 or thick dashed black line in Fig. 7) because a certain amount of supersaturation is required, for nucleation to occur (Koop et al., 2000). Wave cooling would be adiabatic;

it would follow an isentrope (dash-dotted lines) in Figs. 1, 4 and 7, and reach T_{ice} at higher altitude. One possibility would be waves driven by wind shear (Kelvin Helmholtz-instability). But even though the wind shear was quite large (up to 25 (m/s)/km close to 18 km altitude), the Richardson number (de Silva et al., 1996) stays well above 2, which implies that conditions do not allow for evolution of Kelvin Helmholtz-instabilities at this altitude. The most likely source for waves would be the thunderstorms, located 100–200 km away from the observation site. Tropical thunderstorms are known to induce gravity waves (Larsen et al., 1982; Song et al., 2003; Lane et al., 2001). Such gravity waves have periods of a few minutes, e.g. 6 min according to Larsen et al. (1982), and on that time scale sedimentation is insignificant. This implies that condensation and subsequent sublimation would be practically reversible processes, happening on approximately equal time scales. Thus, after a wave train has passed, and the air parcel is left in its initial temperature and pressure state, any particle which might have been formed would sublimate within few minutes, which is the time scale of a wave period, and particles would only be present during the wave passing. In the temperature profile recorded on board the backscatter payload, we find no signature of gravity waves, and therefore the possibility of "wave generated" particles seems unlikely.

In a more likely scenario the particles were lifted into the stratosphere by a distant thunderstorm, accompanied by a large amount of water vapor, and then transported to the point of observation. This hypothesis can be rationalized by a closer inspection of the radar image sequence covering the late afternoon leading up to the measurements. Trajectories calculated from the ECMWF operational analysis lead to a group of thunderstorms in the South Atlantic Convergence Zone 200–240 km east-northeast of Bauru 5–6 h earlier (Figs. 2 and 3). Exploring different combinations of particle fall-speeds and trajectory starting points, it turns out that the forward trajectories calculated from a specific thunderstorm at 16:46 local time (19:46 UT 20 February), 215 km E.N.E. from Bauru, hits the point of observation (01:20 UT 21 February) when the particles were observed. The match can be obtained with different combinations of start-altitudes and particle fall speed. Fall speeds in the range 0.0–0.1 m/s were tested,

corresponding to particle radii of 0–17 μm. A fall speed of 0.028 m s^{-1} is chosen as an example and shown in Figs. 2 and 3. A manual inspection of echo tops at the –5 dBZ radar reflectivity threshold shows that the storm turret goes up to at least 19.4 km. There may have been more ice crystals above this height, but due to the long range (>200 km) and their low concentration, they would have been below the detection limit of the Bauru radar. Assuming that the particles were composed of ice, they could not be much larger, since they would have to reside in air masses which were saturated or supersaturated with respect to ice during the process in order not to sublimate within a few minutes (Larsen, 1992). This means that the particles would have to stay within humid tropospheric air which entered and mixed with the stratosphere along with the particles, without sedimenting out.

4.2 Mixing process

The ozone profile recorded in situ simultaneously with the aerosol backscattering signal shows no sign of tropospheric values in the air masses close to the observation, which might seem inconsistent with the hypothesized scenario. However, one has to bear in mind that tropospheric air mixed with stratospheric air at a given altitude, will have to descend a certain distance to reach the level of neutral buoyancy (Danielsen, 1982). Let α be the fraction of tropospheric air, and $(1-\alpha)$ the fraction of stratospheric air in the mixed air parcel. Assuming adiabatic transport and no chemical O_3 production we can write two different relations for the mixing process

$$\chi_t \alpha + \chi_s(1-\alpha) = \chi_m \quad (1)$$

$$\theta_t \alpha + \theta_s(1-\alpha) = \theta_m, \quad (2)$$

where θ is the potential temperature, χ the ozone mixing ratio, and the subscripts t, s and m refer to "tropospheric", "stratospheric" and "mixed" air. While Eq. 1 is self explaining, 2 is achieved by considering the physical process of mixing: When two air parcels, t and s, of respective mass coefficients α and $(1-\alpha)$ and potential temperatures θ_t and θ_s, mix they must be transported to the same pressure level. Here we

assume that this happens through an adiabatic ascent of tropospheric air (t), i.e., the potential temperatures of the two air parcels are conserved. As they reach the same pressure p, their potential temperatures are given by $\theta_t = T_t \left(\frac{p_0}{p}\right)^{\kappa}$ and $\theta_s = T_s \left(\frac{p_0}{p}\right)^{\kappa}$, where $\kappa = R/c_p$. After the mixing process the potential temperature is determined by the temperature of the mix: $\theta_m = (\alpha T_t + (1-\alpha)T_s)\left(\frac{p}{p_0}\right)^{\kappa} = \alpha\theta_t + (1-\alpha)\theta_s$, which is simply a weighted mean of their respective potential temperatures. Actually the rising air parcel looses some of its water vapor content during the process due to condensation, so formally one should use the equivalent potential temperature instead of θ to form relation 2, but the role of condensation in terms of heating is insignificant due to low water vapor content in the TTL. It is not possible to close the Eqs. 1 and 2, but from the linearity between ozone and potential temperature in the lower stratosphere (see Fig. 8) we can reduce the number of unknowns to only three in Eqs. (1) and (2). This enables us to deduce a relation between the potential temperature θ_t at the altitude where the tropospheric air originates, and the tropospheric air mixing coefficient α. The relation is plotted as a thick red area in Fig. 8. If the entraining air came from below the lapse rate tropopause at 15 km (θ=352 K), we can estimate that the mixed air is composed of 1/5 tropospheric air, and 4/5 stratospheric air. The turret must have reached an altitude of at least 19.7 km (θ=462 K) in order to obtain neutral buoyancy at 18.9 km. It can be seen from Fig. 3 that the storm C1 exceeded 20 km in height, thus confirming this rationale.

4.3 Turret altitude

The observation of particles on 21 February 2004, 01:19 UT at 17.7 to 18.9 km can be rationalized if deep convection can go up to at least 19.7 km. In the literature there are several observations of turrets reaching this altitude (Alcala and Dessler, 2002; Adler and Mack, 1986; Ebert and Holland, 1992; Simpson et al., 1993). As shown in Sect. 2, the situation for the 14 February 2001 observation was very similar. It will be up to

future campaigns to possibly confirm and explore such events.

4.4 Hydration

At the time when the tropospheric air was lifted through the TTL it must have been cooled considerably; thus, it had to carry practically all the water that it contained at the observation time as ice particles. Assuming that the air surrounding the particles was saturated at the observation time we can asses the total water content: The gas phase water mixing ratio q_{vap} is calculated from the temperature at 18.9 km altitude (see Fig. 1), and the solid phase water mixing ratio is estimated by assuming that the ice particle median radius is 1 μm, (the exact size does not matter for this purpose since most water is found to be in the gas phase) $q_{tot}=q_{vap}+q_{ice}=2.2\times10^{-5}+4\times10^{-8}$ kg (kg air)$^{-1}$. Assuming now that the tropospheric and stratospheric air were mixed with the ratio 1:4, as estimated in Sect. 4.2, it follows that the number density in the entraining tropospheric air must have been at least 5 times 0.4-10$\times10^{6}$ (kg air)$^{-1}$ (5 times the number density interval estimated in Sect. 3). Likewise the total water content must have been larger than q_{tot}, approximately 1.0×10^{-4} kg (kg air)$^{-1}$, in the entraining tropospheric air. Distributed equally among the present particles, it leads to a particle radius of 7–23 μm at the time of detrainment from the convection turret. This number is highly uncertain, since larger particles may have settled out of the mixed air parcel, and smaller particles may have sublimated. It would correspond to a vertical velocity of at least 0.01 to 0.1 m s^{-1} in order to lift the particles, which is easily achieved.

If the particles were composed of ice, which we have argued is the most likely case (Sect. 3), there is no doubt that the studied overshoot effectively hydrated the stratosphere. During the detraining process, when the air masses were mixed, ice particles lost most of their water content by sublimation, and the ice particles, which were still present at the observation time, were bound to sublimate in the lower stratosphere as they sedimented out of their saturated environment, or as their environment was further diluted with dryer stratospheric air. Eventually the intruded water would be brought fur-

ther into the stratosphere due to Brewer Dobson circulation. We note, that even though the rareness of turrets penetrating deep into the lower stratosphere leaves little potential for dehydration, they may actually have larger hydration potential. For example in the case discussed above, the intruding air masses had water contents which were more than an order of magnitude larger than the typical stratospheric air, and thus had ability to hydrate a large airmass. In the other observation, O2, the lidar backscatter ratio at 532 nm is twice as large (consequently the equivalent backscatter ratio at 940 nm would be even larger) and the particles were found at slightly higher altitude. In other respects the signatures of the two observations are quite similar, so there is reason to assume that O2 is also an indication of hydration of the lower stratosphere. The importance of this kind of process for the stratospheric water vapor budget cannot be deduced without knowledge about the frequency of such deep convective events.

Held et al. (2003) studied the frequency of radar echoes at the 10 dBZ reflectivity threshold penetrating through the tropopause during a seven-year period of the month February. They found, that at least one or more storms within the 240 km radar range reached the lower stratosphere on an average of 33% of the days, with a maximum frequency of more than 50% during February 1998 and 1999. Subsequently, Gomes and Held (2004) studied the echo top (10 dBZ radar reflectivity) distribution of storms during a ten-year period found and that 17% of all storms within the 240 km radar range exceeded 15 km, commonly reaching up to 17–19 km a.m.s.l. In a global satellite based study Liu and Zipser (2005) reports a maximum occurrence of overshooting cloud tops (altitude ≈420 K) over continents, with a local maximum frequency over Southern Brazil in December to February. According to the authors, their estimate of 0.005% total overshooting area is an underestimate due to their 20 dBZ reflectivity threshold. It would be premature, at this stage, to quantify the impact of these very deep convective events on the stratospheric water budget, without more information about their frequency and their microphysics.

We cannot rule out the possibility that the particles were partly composed of NAT. There are several possibilities for the internal particle structure. For example, one

possibility would be that the particles were composed of an ice kernel coated with NAT, implying that they would not need to reside in air saturated with respect to water vapor over ice or NAT. If this is the case, we cannot be that specific about the water content of the air surrounding the particles, since we do not know its thermodynamic history. It is too speculative to elaborate further on such details with the information that we have at hand. However, we can conclude that the intruding air must act hydrating rather than dehydrating to the lower stratosphere, due to the water bound in ice and NAT, though the hydration potential is unknown.

Although we cannot decide whether we observed NAT or ice particles, we conclude that O1 and O2 are signatures of hydration.

4.5 Further observations

Finally, we would like present a striking observation of large amounts of water vapor above the TTL achieved during the HIBISCUS campaign, which could be a further evidence for the presence of solid particles in the lower stratosphere. There are certain reservations to this measurement due to potential instrumental artifacts. Nevertheless we believe it is worthwhile mentioning these unusual H2O observations to support the discussion, with the caveat, of the instrumental reservations clearly explained here, kept in mind. It is important to emphasize that our conclusions from the particle measurements are completely independent of this observation.

Four days after O1, on 24 February 2004, 22:00 UT, a water vapor profile was measured in situ from Bauru by the balloon borne micro-SDLA sensor. The H2O concentration was determined in situ during the descent of the gondola by diode laser absorption spectroscopy at 1.39 micron with an inaccuracy of a few percent and a temporal resolution of four samples per second (Durry et al., 2004). A complete discussion of the micro-SDLA H2O data in the UT and the TTL is presented in companion papers elsewhere in the same special issue of ACP. We focus here on the upper part of the flight above the TTL, where a surprisingly high water vapor concentration was observed during the descent of the balloon as reported in Fig. 9. The water vapor mixing ratio

increases from 5 ppmv at 18.5 km to 9–10 ppmv at 20 km, which is far above the usual values of 5 ppmv expected in the lower stratosphere. The flight happened under meteorological conditions quite similar to those of O1, as is seen from Fig. 10. The large amounts of water are likely due to humid tropospheric air being advected with a northeasterly flow from a Cyclonic Vortex at High Altitude located over the coastal region of Northeast Brazil (State of Bahia), and entering the stratosphere by deep convection, as confirmed by observations from the Bauru radar.

Nonetheless, a competing explanation for this observation is pollution of the measurement by water vapor out-gassing from the balloon envelope at the beginning of the slow descent where it is known that the balloon may oscillate a little (Durry and Megie, 2000; Durry et al., 2002) until the descent speed has stabilized. Nevertheless, in the HIBISCUS flights, the descent was achieved with a day-to-night transition (the balloon temperature decreases at sunset initiating thereby the slow descent), instead of using a valve. This results in a much more smooth slow descent with little oscillations. Hence, we have not observed the usual spikes of water vapor which indicates the vertical oscillations of the balloons (Durry et al., 2002). There is no further clear evidence of contamination from the examination of the GPS information and temperature data. Furthermore, for the HIBISCUS flights, small balloons (3000 m3) were used to carry the micro-SDLA up to 22 km, instead of the usual large balloons (50 000 m3) implemented to probe the stratosphere. A smaller diameter of the balloon strongly reduces the corruption effect. Therefore, the issue of the significance of these striking large amounts of water vapor is still open. We believe that it could be residues of deep convection where humid tropospheric air masses are mixed with stratospheric air. The conditions are present for this to be the case. As shown in Fig. 10 there was a lot of convective activity east of Bauru in the afternoon, and with the easterly around 18–20 km, shown with arrows, it is very likely, that overshooting air was transported over Bauru during the evening.

5 Conclusions

In two cases during the HIBISCUS campaigns solid particles were observed at very high altitudes in the lower stratosphere in the South Atlantic Convergence Zone. These observations indicate that deep convection can reach altitudes of at least up to 20.8 km. In one of the observations it was possible to make a rough estimate of the particle radii to be in the order of 0.2–1.5 μm, and the number density to be 0.03–1 cm^{-3}. In the other observation it could be concluded that the particles where solid. Through a study of the local meteorological situation it was in one case concluded that the air mass where the particles occur was most likely originating from a specific thunderstorm seen in radar images 5.5 h before the observation, and that it must have carried a considerable amount of ice-water into the stratosphere to maintain saturation of water vapor with respect ice while mixing with stratospheric air. We have argued that due to their estimated size and number density, the particles were most likely composed of ice, which implies that airmasses with a total water vapor mixing ratio of at least 160 ppmv entered the stratosphere along with the particles. No matter whether the particles consisted of pure ice or were partly composed of NAT, we are lead to conclude that their presence is an indication of hydration through deep convection. We find additional evidence for this sort of process in water vapor measurements from the same location, showing enhanced water vapor mixing ratios, up to around 10 ppmv, in the lowest stratosphere during similar meteorological conditions.

Acknowledgements. We would like to thank A. Garnier (CNRS) and the rest of the HIBISCUS team. We also thank the coordinators of the TroCCiBras Project and the IPMet staff for providing the infrastructure support during the campaign. This work was supported by the Danish National Space Board (OFR), the EC project HIBISCUS and the integrated EC project SCOUT-O3. One of the authors, J. M. Rosen, was supported by the U.S. National Science Foundation.

References

Adler, R. F. and Mack, R. A.: Thunderstorm Cloud Top Dynamics as Inferred from Satellite Observations and a Cloud Top Parcel Model, J. Atmos. Sci., 43, 1945–1960, 1986. 9006, 9013

Alcala, C. M. and Dessler, A. E.: Observations of deep convection in the tropics using the Tropical Rainfall Measuring Mission (TRMM) precipitation radar, J. Geophys. Res. (Atmos.), 107(D24), 4792, doi:10.1029/2002JD002457, 2002. 9006, 9013

Danielsen, E. F.: A dehydration mechanism for the stratosphere, Geophys. Res. Lett., 9, 605–608, 1982. 9005, 9012

de Silva, I. P. D., Fernando, H. J. S., Eaton, F., and Hebert, D.: Evolution of Kelvin-Helmholtz billows in nature and laboratory, Earth Planet. Sci. Lett., 143, 217–231, 1996. 9011

Di Donfrancesco, G., Cairo, F., Buontempo, C., Adriani, A., Viterbini, M., Snels, M., Morbidini, R., Piccolo, F., Cardillo, F., Pommereau, J. P., and Garnier, A.: Balloonborne lidar for cloud physics studies, Appl. Opt., 5701–5708, 2006. 9008

Durry, G. and Megie, G.: In situ measurements of H2O from a stratospheric balloon by diode laser direct-differential absorption spectroscopy at 1.39 μm, Appl. Opt., 39, 5601–5608, 2000. 9017

Durry, G., Hauchecorne, A., Ovarlez, J., Ovarlez, H., Pouchet, I., Zeninari, V., and Parvitte, B.: In situmeasurement of H2O and CH4 with telecommunication laser diodes in the lower stratosphere: dehydration and indication of a tropical air intrusion at mid-latitudes, J. Atmos. Chem., 43, 175–194, 2002. 9017

Durry, G., Amarouche, N., Zninari, V., Parvitte, B., Lebarbu, T., and Ovarlez, J.: In situ sensing of the middle atmosphere with balloonborne near-infrared laser diodes, Spectrochim. Acta A, 60, 3371–3379, 2004. 9016, 9031

Ebert, E. E. and Holland, G. J.: Observations of Record Cold Cloud-Top Temperatures in Tropical Cyclone Hilda (1990), Monthly Weather Rev., 120, 2240–2251, 1992. 9006, 9013

Folkins, I., Loewenstein, M., Podolske, J., Oltmans, S. J., and Proffitt, M.: A barrier to vertical mixing at 14 km in the tropics: Evidence from ozonesondes and aircraft measurements, J. Geophys. Res., 104, 22 095–22 102, 1999. 9005

Fueglistaler, S., Wernli, H., and Peter, T.: Tropical troposphere-to-stratosphere transport inferred from trajectory calculations, J. Geophys. Res. (Atmos.), 109, D3108, doi:10.1029/2003JD004069, 2004. 9005, 9006

Gettelman, A., Holton, J. R., and Douglass, A. R.: Simulations of water vapor in the lower stratosphere and upper troposphere, J. Geophys. Res. (Atmos.), 105, 9003–9024, 2000. 9005

Gomes, A. M. and Held, G.: Determinação e avaliação do parâmetro densidade VIL para alerta de tempestades., in XIII Congresso Brasileiro de Meteorologia, 29 August–3 September, 12pp, SBMET, Fortaleza, 2004. 9015

Hartmann, D. L., Holton, J. R., and Fu, Q.: The heat balance of the tropical tropopause, cirrus, and stratospheric dehydration, Geophys. Res. Lett., 28, 1969–1972, 2001. 9005

Held, G., Gomes, A. M., and Figuiredo, J. C.: Statistics of echo top and VIL density and local synoptic situations in São Paolo State, in TROPIC Workshop, Wessling 14–16 May 2003, http://www.pa.op.dlr.de/troccinox/private/meetings/TROPIC/, 2003. 9015

Holton, J. R. and Gettelman, A.: Horizontal transport and the dehydration of the stratosphere, Geophysical Research Letters, 28, 2799–2802, 2001. 9005

Holton, J. R., Haynes, P. H., McIntyre, M. E., Douglass, A. R., Rood, R. B., and Pfister, L.: Stratosphere-troposphere exchange, Rev. Geophys., 33, 403–439, 1995. 9004

Jensen, E. and Pfister, L.: Transport and freeze-drying in the tropical tropopause layer, J. Geophys. Res. (Atmos.), 109, D2207, doi:10.1029/2003JD004022, 2004. 9006

Jensen, E., Pfister, L., Ackerman, A., and Toon, O.: A conceptual model of the dehydration of air due to freeze-drying by optically thin, laminar cirrus rising slowly across the tropical tropopause, J. Geophys. Res., 106(d15), 17 237–17 252, 2001. 9005

Koop, T., Luo, B., Tsias, A., and Thomas, P.: Water activity as the determinant for homogeneous ice nucleation in aqueous solutions, Nature, 406, 611–614, 2000. 9010

Küpper, C., Thuburn, J., Craig, G. C., and Birner, T.: Mass and water transport into the tropical stratosphere: A cloud-resolving simulation, J. Geophys. Res. (Atmos.), 109, D10111, doi:10.1029/2004JD004541, 2004. 9005

Lane, T. P., Reeder, M. J., and Clark, T. L.: Numerical Modeling of Gravity Wave Generation by Deep Tropical Convection., J. Atmos. Sci., 58, 1249–1274, 2001. 9011

Larsen, M. F., Swartz, W. E., and Woodman, R. F.: Gravity-wave generation by thunderstorms observed with a vertically-pointing 430 MHZ radar, Geophys. Res. Lett., 9, 571–574, 1982. 9011

Larsen, N.: Stratospheric Aerosols, Tech. rep., Danish Meteorological Institute, 1992. 9012

Liu, C. and Zipser, E. J.: Global distribution of convection penetrating the tropical tropopause, J. Geophys. Res. (Atmos.), 110, D23104, doi:10.1029/2005JD006063, 2005. 9015

Mishchenko, M. I. and Travis, L. D.: Capabilities and limitations of a current FORTRAN implementation of the T-matrix method for randomly oriented, rotationally symmetric scatterers – Computational Methods, J. Quant. Spectrosc. Radiat. Transfer, 60, 309–324, 1998. 9008

Newell, R. E. and Gould-Stewart, S.: A Stratospheric Fountain?., J. Atmos. Sci., 38, 2789–2789, 1981. 9004

Pommereau, J.-P.: HIBISCUS Homepage, http://www.aerov.jussieu.fr/projet/HIBISCUS/en/many/index.html, 2004. 9006

Popp, P. J., Marcy, T. P., Jensen, E. J., Kaercher, B., Fahey, D. W., Gao, R. S., Thompson, T. L., Rosenlof, K. H., Richard, E. C., Herman, R. L., Weinstock, E. M., Smith, J. B., May, R. D., Voemel, H., Wilson, J. C., Heymsfield, A. J., Mahoney, M. J., and Thompson, A. M.: The observation of nitric acid-containing particles in the tropical lower stratosphere, Atmos. Chem. Phys., 6, 601–611, 2006. 9009

Potter, B. E. and Holton, J. R.: The Role of Monsoon Convection in the Dehydration of the Lower Tropical Stratosphere, J. Atmos. Sci., 52, 1034–1050, 1995. 9005, 9010

Rosen, J. M. and Kjome, N. T.: Backscattersonde - A new instrument for atmospheric aerosol research, Appl. Opt., 30, 1552–1561, 1991. 9007

Schreiner, J., Voigt, C., Weisser, C., Kohlmann, A., Mauersberger, K., Deshler, T., Kröger, C., Rosen, J., Kjome, N., Larsen, N., Adriani, A., Cairo, F., Di Donfrancesco, G., Ovarlez, J., Ovarlez, H., and Dörnbrack, A.: Chemical, microphysical, and optical properties of polar stratospheric clouds, J. Geophys. Res. (Atmos.), 108, D5, 8313, doi:10.1029/2001JD000825 2003. 9008

Sherwood, S. C. and Dessler, A. E.: A Model for Transport across the Tropical Tropopause, J. Atmos. Sci., 765–779, 2001. 9005

Simpson, J., Keenan, T. D., Ferrier, B., Simpson, R. H., and Holland, G. J.: Cumulus Mergers in the Maritime Continent Region, Meteorol. Atmos. Phys., 51, 73–99, 1993. 9006, 9013

Song, I.-S., Chun, H.-Y., and Lane, T. P.: Generation Mechanisms of Convectively Forced Internal Gravity Waves and Their Propagation to the Stratosphere., J. Atmos. Sci., 60, 1960–1980, 2003. 9011

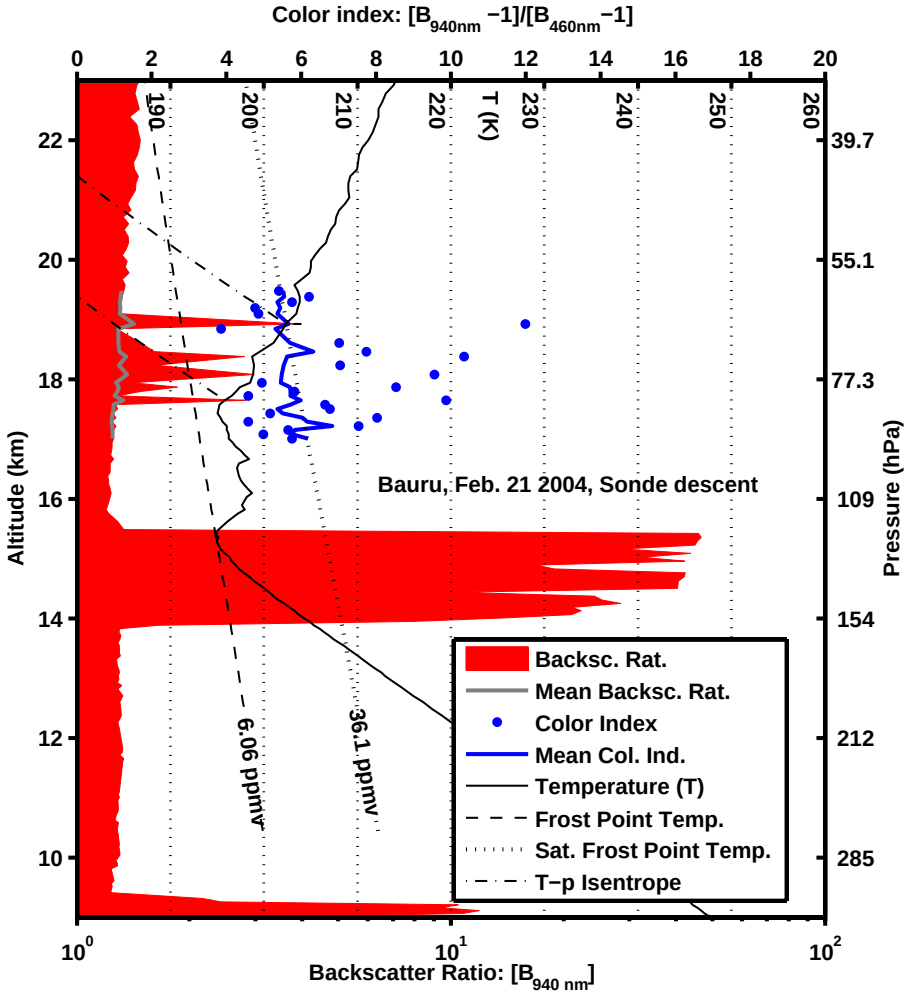
Color index: [B940nm −1]/[B460nm −1]
0
2
4
6
8
10
12
14
16
18
20
190
200
210
220
T (K)
230
240
250
260
22
20
18
16
14
12
10
39.7
55.1
77.3
109
154
212
285
Altitude (km)
Pressure (hPa)
Bauru, Feb. 21 2004, Sonde descent
Backsc. Rat.
Mean Backsc. Rat.
Color Index
Mean Col. Ind.
Temperature (T)
Frost Point Temp.
Sat. Frost Point Temp.
T−p Isentrope
6.06 ppmv
36.1 ppmv
10^0
10^1
10^2
Backscatter Ratio: [B940 nm]

Fig. 1.

Fig. 1. O1. Backscatter sounding recorded at 21 February 2004 01:00 to 02:00 on descent, at 49.03 W 22.36 S. Red filled function: Backscatter ratio at 940 nm ($B_{940\,\mathrm{nm}}$). The backscatter ratio is given by $S=(B_R+B_A)/B_R$, where B_R is the molecular backscatter coefficient, and B_A is the aerosol backscatter coefficient. Thick grey curve: Average backscatter ratio for all flights (including both ascent and descent). The whole series counts 10 flights, launched in February 2004 from the same location. Blue dots: Color index (i.e., $\frac{B_{940\,\mathrm{nm}}-1}{B_{480\,\mathrm{nm}}-1}$) for 21 February flight. Thick blue curve: Average color index for all soundings. Thin black curve: Temperature (K). Dashed black curve: Estimate of frost point temperature (T_{ice}). T_{ice} is estimated from the flight temperature and pressure data by assuming saturation of water vapor with respect to ice at all altitudes (an overestimate), and then finding the minimum water vapor mixing ratio. In this case a water vapor mixing ratio minimum of 6.06 ppmv is found at 15.3 km, and this mixing ratio is used to calculate T_{ice}. The dotted black curve is the frost point temerature calculated by assuming a water vapor mixing ratio of 36.1 ppmv, corresponding to saturation with respect to ice at the highest altitude with particle occurrence. The dash-dotted curves marks the isentropes which would have to be followed if air is cooled through expansion.

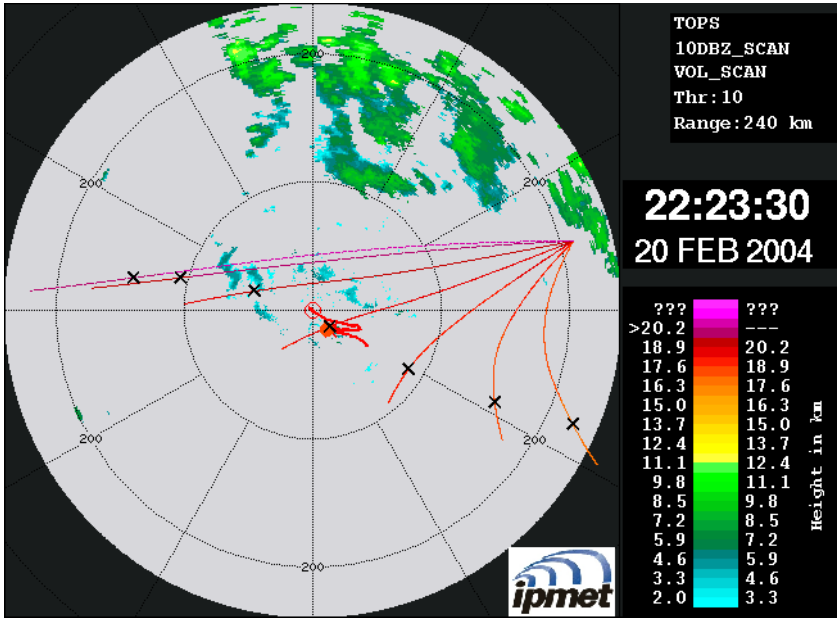

Fig. 2. O1. Radar image of echo top altitude (10 dBZ radar reflectivity threshold) observed at the time when the particles were observed. The balloon (red thick trajectory) was launched at the location of the Bauru Radar (center). The radar range is 240 km. There are no convective cells in the vicinity of the observation. The multi colored lines are trajectories, derived from ECMWF operational analysis, initiated approximately at the center of a storm 5.5 h before the observation, at altitudes 18.5, 18.9, 19.4, 19.9, 20.5, 21.1, and 21.8 km. A fall speed of 0.028 m/s, corresponding approximately to a particle radius of 10 μm, is assumed. The color shading of the trajectories indicates the altitude according to the same scale as the echo top. The red filled bullet indicates the observation point.

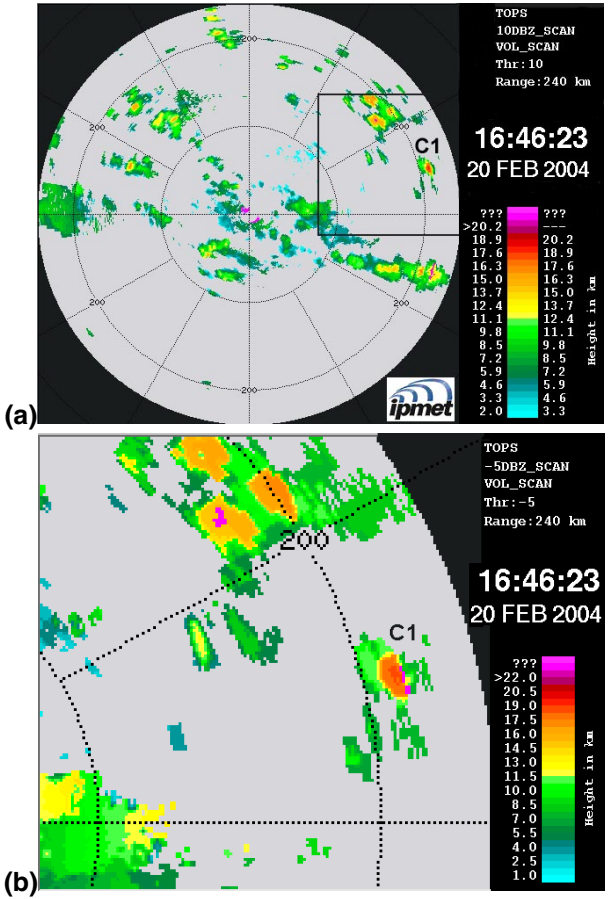

Fig. 3. **(a)** Same as in Fig. 2, 5 h and 37 min earlier. **(b)** Enlargement of the area from which the sampled airmasses originate. This map is made with a −5 dBZ radar reflectivity threshold.

ACPD
6, 9003–9032, 2006

EGU

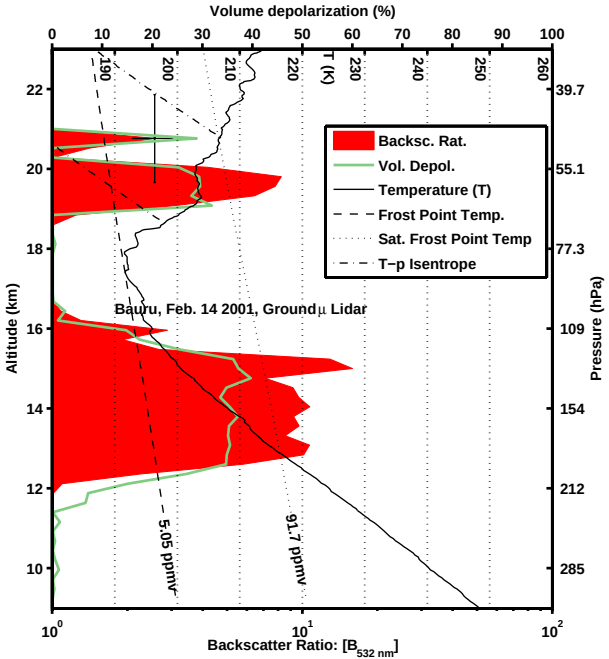

Fig. 4. O2. Backscatter data recorded with the 532 nm μ-Lidar from ground on 14 February 2001, at 49.03 W 22.36 S. Filled red function: Backscatter ratio (same parameter as in Fig. 1, just another wavelength). Green curve: Volume depolarization $\frac{B_{\perp}}{B_{\parallel}}$ (perpendicular component divided by parallel component of backscattering signal), where $B{=}B_R{+}B_A$ is the sum of molecular and aerosol backscattering coefficients. The backscatter signals from high altitude were present for approximately 15 min, and the plots represent averages over this time interval. Thin black curve: Temperature recorded on February 13 22:00 UT. Dashed black curve: Frost point temperature calculated in the same manner as in Fig. 1. Dotted black curve: Frost point temperature calculated by assuming a water vapor mixing ratio of 91.7 ppmv, corresponding to saturation with respect to ice at the highest altitude of particle occurrence. The dash-dotted curves mark the isentropes which have to be followed if air is cooled through expansion.

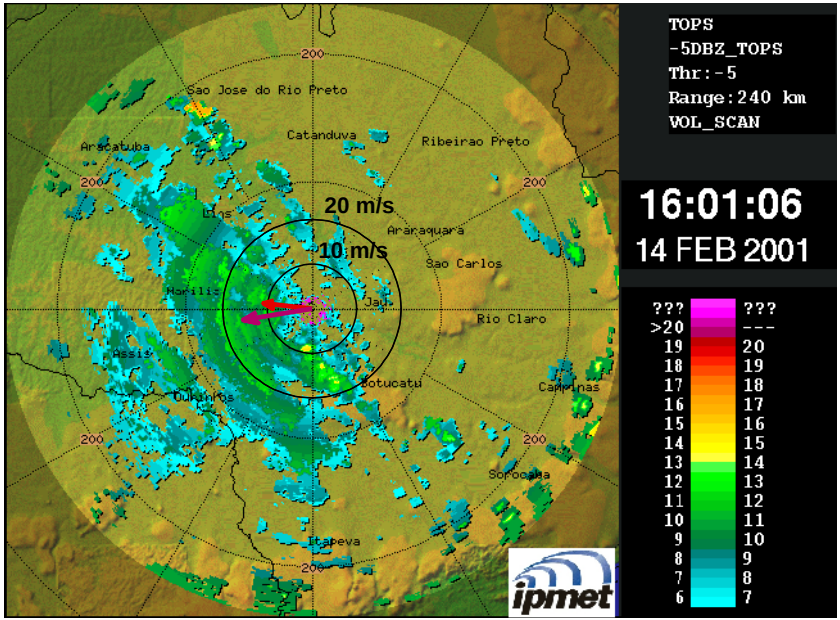

Fig. 5. O2. Radar image of echo top altitude (−5 dBZ radar reflectivity threshold) observed at 16:01, local sun time, on 14 February 2001 from Bauru. The radar range is 240 km. Note the area of convective activity in the eastern part of the radar range. The arrows in the center show the ECMWF operational analysis wind over Bauru on 14 February 2001, 15:00 local time, at 17, 19 and 21 km altitude (their color refers to the same colorbar as the cloud top altitudes). Please note that the inner circles of the polar grid delineate the wind speed in m/s, while the outer circles indicate distance from the Bauru radar in km.

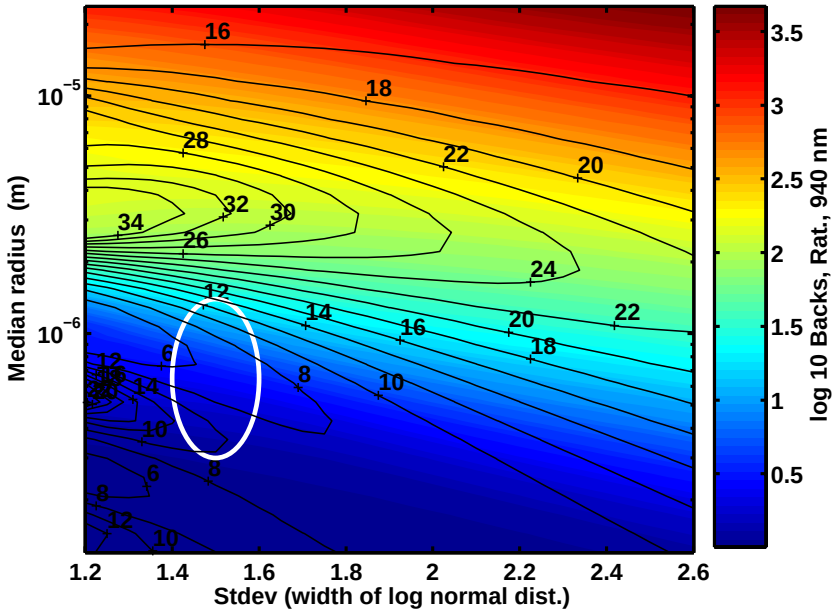

Fig. 6. Backscattering parameters for different log-normal size distributions characterized by their median radius, and width (stdv). Color map: Backscatter ratio $B=(B_R+B_A)/B_R$ at 940 nm. Black contours: Color index $\frac{B_{940\,\mathrm{nm}}-1}{B_{480\,\mathrm{nm}}-1}$. Properties are calculated for assumed particle density of 10^6 particles per kg air, temperature 200 K, and pressure 100 hPa. The area inside the white ellipse indicates a reasonable guess of the log-normal parameters, guided by the observed color index.

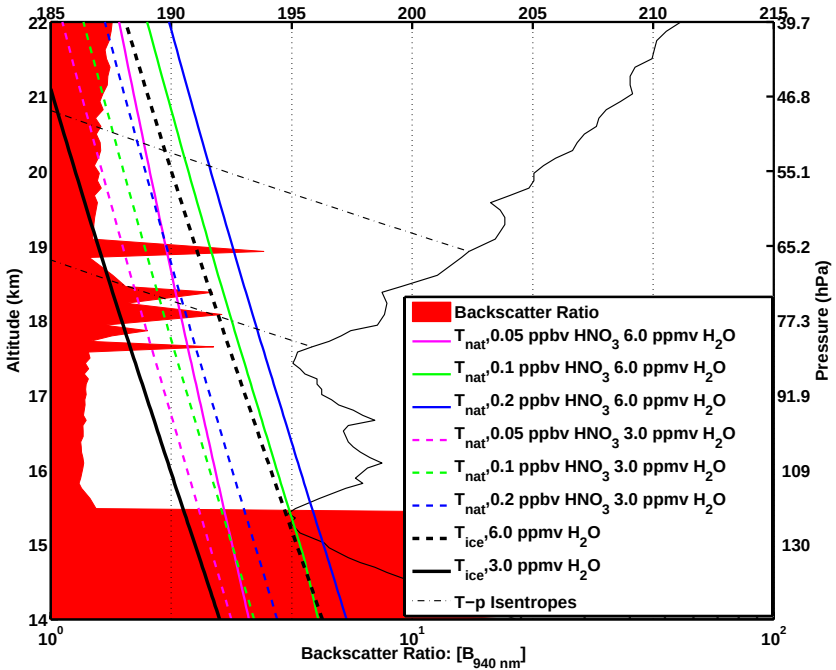

Fig. 7. Filled red curve: Backscattering Ratio as in Fig. 1. Colored curves: Condensation temperatures for NAT. Thick black curves: Condensation temperatures for ice (Frost point temperatures). See legend for different assumptions about water and HNO_3 gas phase mixing ratio. Thin black curve: Temperature as in Fig. 1 and thin dot-dashed curves: Isentropes calculated from the pressure profile.

ACPD
6, 9003–9032, 2006

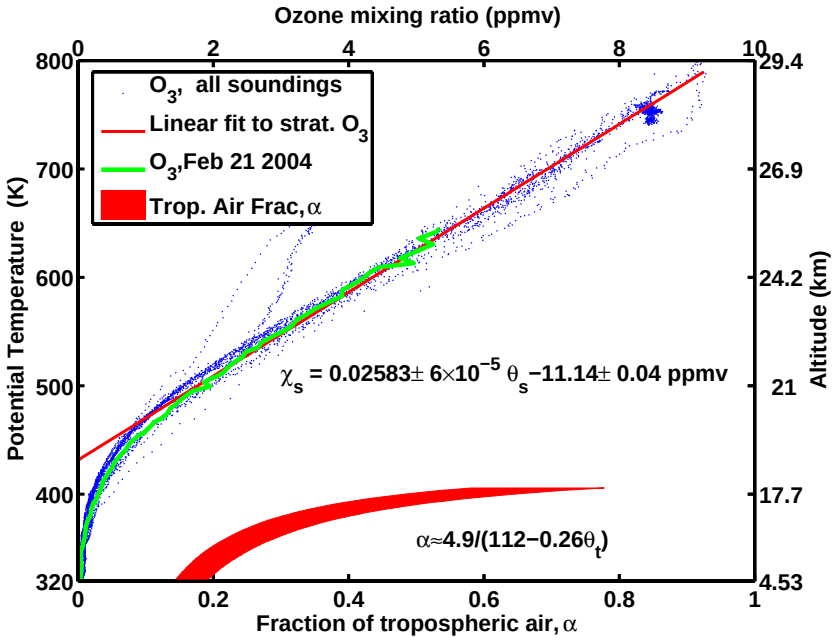

Fig. 8. Blue dots: Scatter plot of Potential Temperature versus Ozone Volume Mixing Ratio measured through 10 independent soundings over Bauru in February 2004. Ozone mixing ratio depends linearly on potential temperature between 450 and 750 K. Red curve: Linear fit to lower stratospheric ozone. Thick red area: Tropospheric air mixing coefficient calculated by assuming that tropospheric air is originating from different altitudes. The width of the area indicates the uncertainty of the estimated α – value, calculated by propagating the standard errors off the line coefficients in the $\chi - \theta$ relation, through the solution to Eqs. 1 and 2.

ACPD
6, 9003–9032, 2006

EGU

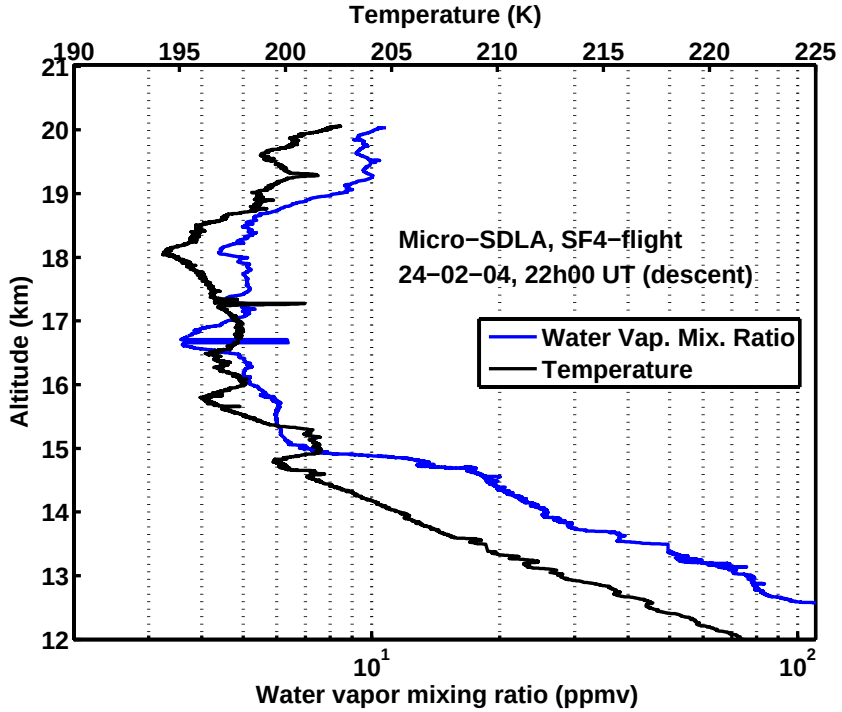

Fig. 9. The H2O vertical mixing ratio profile measured in situ by the micro-SDLA balloon borne diode laser spectrometer (Durry et al., 2004) from Bauru on 24 February 2004 during the HIBISCUS campaign. Large amounts of water vapor were surprisingly observed above the TTL in the 18.5 km to 20 km altitude region. Possibly these large amounts of H2O could be remnants of humid tropospheric air injected by deep convection into the lower stratosphere. See text for more details.

ACPD
6, 9003–9032, 2006

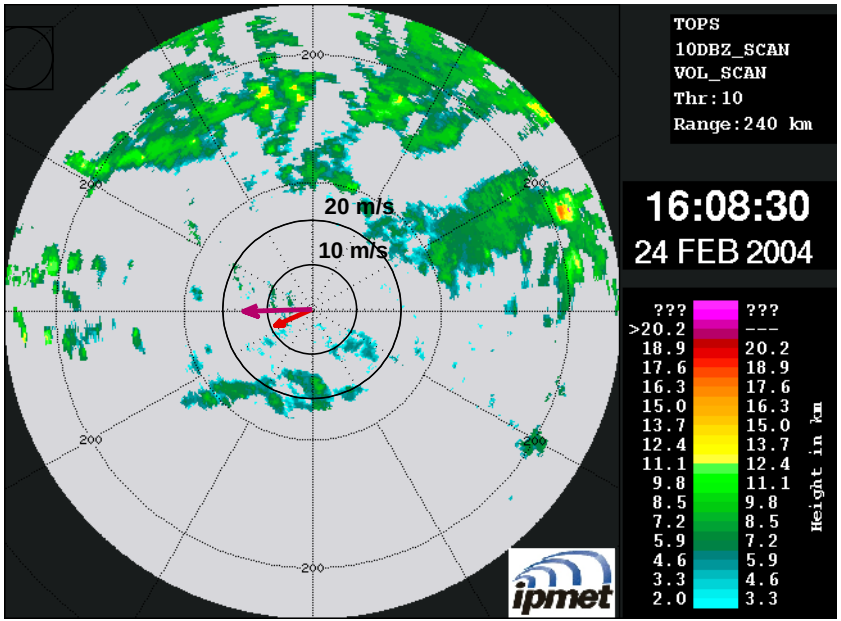

Fig. 10. A snapshot of the cloud top altitude recorded from the Bauru radar late afternoon 6 h before the water vapor mixing ratio profile in Fig. 9 was observed. There is plenty of deep convection going on east of Bauru, and only a small fraction of it is within the radar image. The inserted arrows show the wind field at 17, 19 and 21 km, over Bauru, from ECMWF operational analysis. Please note that the inner circles of the polar grid delineate the wind speed in m/s, while the outer circles indicate distance from the Bauru radar in km. In fact the convective overshoot from which the probed air originates may well be located outside the radar range.